Free water table area monitoring on wetlands using satellite and UAV orthophotomaps – Kampinos National Park case study

Maciej Góraj, Cezary Wróblewski, Wojciech Ciężkowski, Jacek Jóźwiak, Jarosław Chormański
Warsaw University of Life Sciences, Faculty of Civil and Environmental Engineering, Nowoursynowska 159, 02-776 Warsaw, Poland

Abstract. The surface water table level is a crucial factor for the existence of wetland habitats, and valuable from the point of view of environmental protection. In particular, surface water table in a hydrological year play an important role, affecting the seasonal changes in conditions of the development of species inhabiting a given patch of vegetation. The occurrence of floods often determines the possibility of survival of a given plant community.
Information on the seasonal variability of surface waters, and above all the range of seasonal floods, is very important from the point of view of planning protection activities in National Parks in order to preserve wetland habitats.
Nowadays, remote sensing data is an important source of spatial information, particularly those characterized by low cost data acquisition and processing. One such source is imagery collected from satellites, along with products freely distributed by the European Space Agency. Satellites of the Sentinel constellation provide multi-spectral optical remote sensing images recorded at visible and infrared wavelengths. Due to the short satellite revisit time of the Sentinel, the images from this satellite constitute a potential source of information for the monitoring of moisture on wetlands with a high temporal resolution.
In this study, the authors aim to demonstrate the possibilities associated with the use of satellite images to monitor the range of a free surface water table in the pilot area located within the basin of the Łasica Channel, located in the Kampinos National Park (Poland). The accuracy of the results of the remote sensing transformations will be assessed using high resolution RGB images obtained with the use of unmanned aerial vehicles (UAV) and control points measurements. The maps of free water table has been acquired as an result of ensemble regressors (Random Forest, Extra Trees, Bagging). Regressors has been learned and applied for two sessions. Promising results were obtained indicating the possibility of using the proposed method on a similar scale.

Keywords: UAV, Sentinel-2, machine learning, surface water, inundation, wetlands

Submitted 2 May 2018, **revised** 19 July 2018, **accepted** 3 August 2018

1. Introduction

1.1. Fens and hydro-technical constructions

Water dependent habitats, like fens and bogs, play crucial role in a number of important environmental processes, such as water circulation or carbon dioxide accumulation in peat (Wang et al. 2016). Conditions of fen habitats are determined by the seasonal dynamics of the surface water table. Specific bio-societies can be arranged only in terms of the shallow ground water table, which is important from the point of view of organic matter accumulation, and with seasonal floods, which limit less valuable and more common species of drier habitats (Pennings et al. 2004). One of the biggest changes in fen habitats is the anthropogenic modification of rivers in valleys by projecting a channel layout in the plan, for example, the rectification of a channel for water drainage acceleration, or the development of new artificial channels (Gorn et al. 2013). In these cases, fen habitat additional water stress is introduced, and the process of species regression – mainly hydro- and helophytes – begins (Pennings et al. 2004).

1.2. Hydro-technical system in Kampinos National Park

Over the past century, the process of rapid artificial drainage development in Poland has become increasingly popular (Lipiński 2006). This process can be observed in groundwater level course and is observed especially on area of the unique the Kampinos National Park (KPN), which consists of a mosaic of dunes and sensitive wetlands, where ground water level highly influences vegetation distribution and their health status (Piniewski et al. 2012; Kopeć et al. 2013; Krogulec, Zabłocki 2015). The main watercourse (River Łasica) was rectified at the end of the 1960s (Gruszczyński, Krogulec 2012). Before 60s it was a small natural stream which was draining water from local wetlands. After a hydrotechnical reconstruction, this river (named herein Łasica Channel) obtained a simple straight layout. During the period 1969-1998, seven weirs were constructed (Trandziuk 2015). These weirs pile up water during the growing season, thus having an impact on fen habitats as an improving factor (Walker et al. 1994).

1.3. Environmental applications of UAV-borne photogrammetry

Recently, one of the most progressive solutions in photogrammetry is use of UAV (unmanned aerial vehicle) platforms for data acquirement. These platforms allow for data registration within small time periods, with a very high spatial resolution and accuracy, at a relatively low cost (Candiago et al. 2015). They can be applied also at difficult to reach areas (e.g. flooded meadows). Smaller and lighter sensors are becoming available year by year as payloads for UAVs. Such UAV imaging platforms can be applied to many sectors, for example, in precision agriculture (Candiago et al. 2015), thermography and energetic efficiency evaluation (Lagüela et al. 2015), geodetic measurements (Eling et al. 2015), forestry (Torresan et al. 2017) and hydromorphometry (Demarchi et al. 2016).

1.4. Remote sensing techniques for surface water detection

Detection of surface water using remote sensing is a commonly used technique, e.g. McFeeters (1996), Rokni et al. (2014), Jones (2015). The most accurate methods are able to detect not only the surface water table but also groundwater using radar imagery (Jaya, Nagai 2017). Applications also exist that use optical data, raw bands and results of their transformation (such as spectral indices; NDWI, MNDWI, NDMI, etc.) (McFeeters 1996), combining them with PCA transformations for inundation detection, particularly in wetlands areas (Chormański et al. 2011). Theoretically, the latter should constitute a very efficient data source for machine learning, which results from a high discriminant property and the particularly strong proportion between signal and noise (Pereira 1999). Nowadays, low altitude images (including ultralight planes and UAVs) are frequently used. The low altitude allows for a better spatial resolution and accuracy compared to traditional aerial platforms that fly at higher altitudes (Turner et al. 2012). Unfortunately, many of the techniques mentioned are very expensive and cannot be widely used. To overcome this, integrating data with multiple platforms and sensors is key, for example, using free of charge satellite images with small area ground truth images acquired by UAV platforms. With the tools provided by present-day machine learning processes, such as regression based on complex non-linear meta-estimators, it is possible to estimate water table area, with a very high spatial resolution (Gislason et al. 2006).

In this work, the authors want to demonstrate the possibilities associated with the use of remote sensing images recorded from satellite platforms, to monitor the range of a free surface water table in the pilot area located within the basin of the Łasica Channel in the Kampinos National Park. The accuracy of the results of the remote sensing transformations will be assessed using high resolution images obtained with the use of a UAV and ground measurements.

2. Methods and results

2.1. VHR orthophotomap registration and processing

Very high resolution (VHR) photogrammetric images were acquired with a UAV during two field sessions: autumnal (18-21 November 2017) and vernal (14 April 2018). During the autumnal session, flights were made over 5 ground-truth polygons (GTP). During the vernal session, similar flights were made over 3 GTPs (the GTPs 2, 3 and 4 from the autumnal session). All of these GTPs were located in the area of the Kampinos National Park (Fig. 1).

Within each of the GTPs, a geodetic control network (GCN) was developed. The GCN consisted of at least 10 ground control points (GCP). Each GCP was a high contrastive target (chessboard), easy to identify on the acquired images. The location of each GCP was measured using a Topcon GRS-1 GNSS-RTK receiver.

The DJI Phantom 3 Professional UAV was used. It is equipped with an on-board navigation system, including a GNSS receiver, accelerometer, magnetometer and barometer. This navigation system is supported by a visual positioning system (VPS). The UAV is also equipped with a high-resolution RGB camera with a focal length of 3.6 and an effective count of pixels at 12.4 million.

Each flight was executed at 50 m above ground level (AGL), with a velocity equal to 5 m/s. The common overlap of neighboring images was equal to 70% × 70%.

Registered images were processed into RGB orthophotomaps using Agisoft PhotoScan Professional. These products were prepared by a VHR image orthorectification. For this purpose, digital surface models (DSM) were used, obtained using dense-matching.

Obtained orthophotomaps were geometrically calibrated using GCPs. For this purpose, a population of GCPs was split into two subpopulations: Correction GCPs, used for geometrical correction and Validation GCPs, used for the evaluation of the quality of the corrections (Fig. 1).

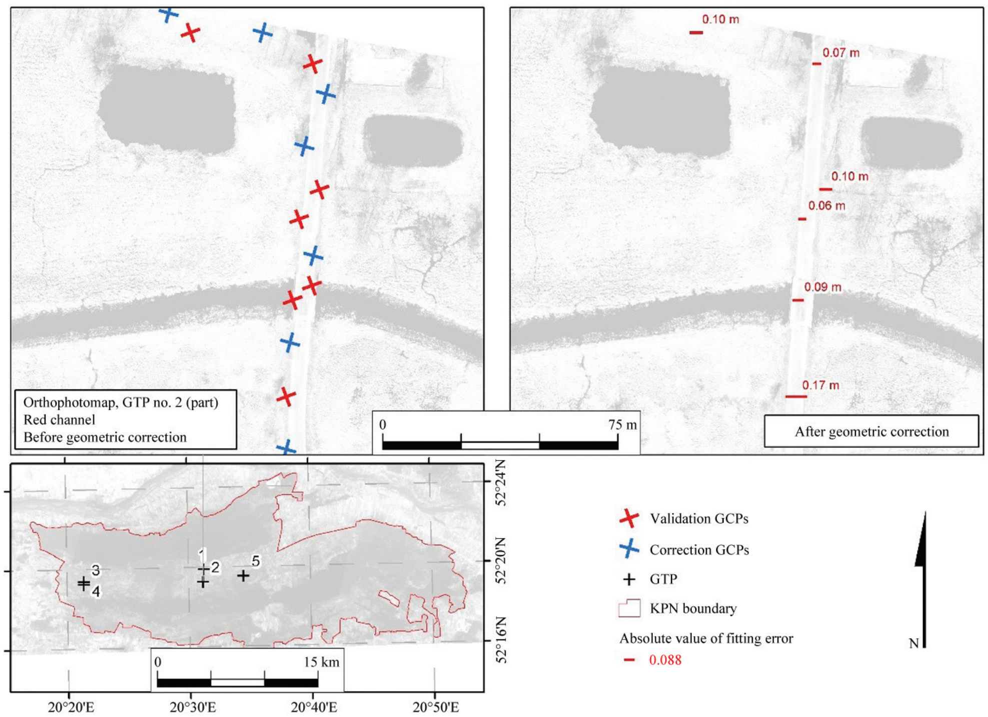

Fig. 1. Geometric correction and validation for GTP polygon no. 2

The resulting products were characterized by mean absolute fitting errors in a range between 0.08 and 0.14 m (Tab. 1). The distribution of GCPs was probably the most important factor affecting this measure.

Table 1. Mean absolute fitting error for GTP polygon orthophotomaps

GTP no.	Session	Mean absolute fitting error [cm]
1	1	0.08
	-	-
2	1	0.12
	2	0.10
3	1	0.13
	2	0.13
4	1	0.14
	2	0.13
5	1	0.11
	-	-

For accurate geometric comparability, the resulting orthophotomaps were resampled into a resolution of 0.05 m/pixel. For this purpose, QGIS implementation of nearest neighbor interpolation algorithm, was used.

2.2. Sentinel-2 image and index preprocessing

Level 2 satellite image products acquired by the Sentinel-2 mission were used (Drusch et al. 2012), with the data being free of charge[1]. Each Sentinel-2 image consists of 13 optical bands, with wavelengths within 0.43-2.28 nm, including the visible (VIS), near infrared (NIR) and short infrared (SIR) bands. Images for the 17th October 2017 and the 10th April 2018 were chosen due to low cloudiness on these days.

Each satellite image was masked into the KPN boundaries. This image was re-projected into the coordinate reference system (CRS) used for the GNSS-RTK and UAV-orthophotomap. The resultant image was characterized by a 10 m/pixel spatial resolution.

The blue (B), green (G), red (R) and NIR bands were selected in order to calculate the normalized difference water index (*NDWI*) (Fig. 2), using the following formula (McFeeters 1996):

$$NDWI = \frac{B3 - B8}{B3 + B8'} \tag{1}$$

where: $B3$ – reflectance for band 3,560.0 nm with FWHM = 45 nm, G band; $B8$ – reflectance for band 3,835.1 nm with FWHM = 145 nm, NIR band.

This index favors areas with a high reflectance in the G band and diminishes in areas with low NIR band reflectances (green but not plants). It has been proven that the *NDWI* is a strong tool for surface water detection (Huang et al. 2015).

Optical bands and *NDWI* datasets were merged and split into the following datasets:

[1] https://scihub.copernicus.eu/dhus/#/home

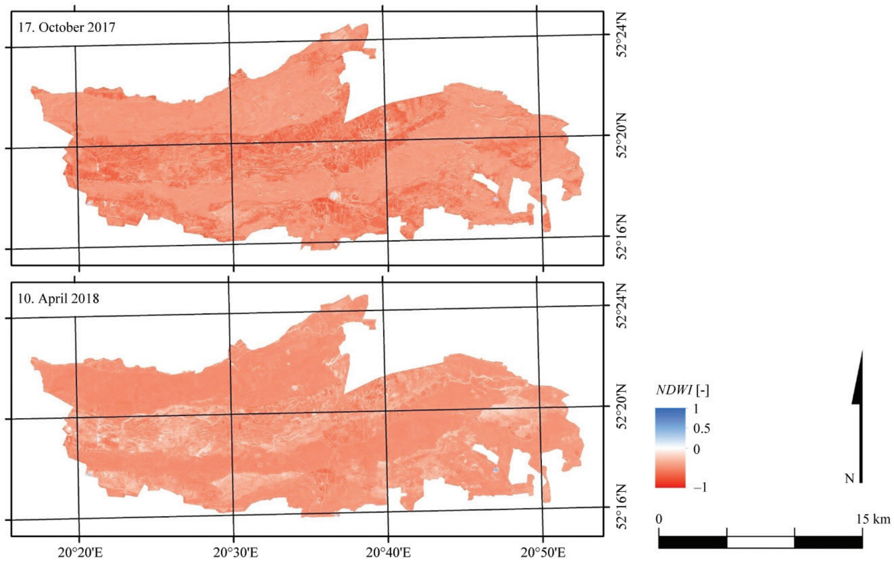

Fig. 2. Derived *NDWI* based on Sentinel-2 optical images

- Set-1: All optical bands;
- Set-2: RGB + NIR;
- Set-3: RGB;
- Set-4: *NDWI*.

2.3. Free water table classification

Photointerpretation was performed on the basis of the VHR orthophotomaps. This consisted of the delineation of reference polygons that are completely covered by water (wet pixels, 1) and completely not covered by water (dry pixels, 0).

Delineated pixels were then split into two subpopulations: classifier training pixels (CTPs) and classifier validation pixels (CVPs). Splitting was prepared into an equal count of pixels (50% × 50%), as the most pessimistic situation in machine learning (high deficiency of observations) yet with a large verification set. Splitting was prepared randomly, with wet/dry classes stratification.

Table 2. Quality indicators of the water table classification

GTP no.	Session	Accuracy	Precision	Recall	F1
1	1	0.997	0.998	0.998	0.998
	-	-	-	-	-
2	1	0.990	0.991	0.991	0.991
	2	0.999	0.999	0.999	0.999
3	1	0.975	0.990	0.731	0.807
	2	0.999	0.999	0.999	0.999
4	1	0.991	0.995	0.994	0.995
	2	0.999	0.999	0.999	0.999
5	1	0.999	0.999	0.999	0.999
	-	-	-	-	-

Using the random forest classifier (RFC), which is accessible via the *scikit-learn* library (Breiman 2001), a two-class classification was made for each GTP. For every outcome, a confusion matrix was calculated.

The outcome of the wet/dry pixel classification is shown in Figure 3, where GTP no. 3 was used. A reduction of the free water table area is visible, primarily in the southern part of the presented GTP (further from the Łasica Channel). For comparison green, the channel brightness wasis shown.

2.4. Percentage of wet VHR pixels regression

Due to the difference in spatial resolution of the VHR orthophotomap (0.05 m/pixel) and the low resolution (LR) Sentinel-2 image (10 m/pixel), the aggregation of VHR pixels was prepared. This was obtained by transforming binary features (wet/dry pixel) into near-continuous features that had a percentage of wet VHR pixels in the LR pixel.

For this purpose, wet LR pixels were counted and divided by the total number of VHR pixels in one LR pixel (size ratio equal to 40 000). This raster data can be interpreted as a surface, where 100% equals 100 m^2 of the free water table.

Using these raster datasets, along with the Sentinel datasets mentioned in the previous chapter (Set-1, …, Set-4), the free water table surface was regressed to the entire KPN. The random forest regressor (RFR), extra trees regressor (ETR) and bagging regressor (BR) were applied as regressors (Breiman 2001; Geurts et al. 2006; Louppe, Geurts 2012). The surface of free water was calculated for both the November and April acquisitions. For this purpose, each combination of two GTPs, from

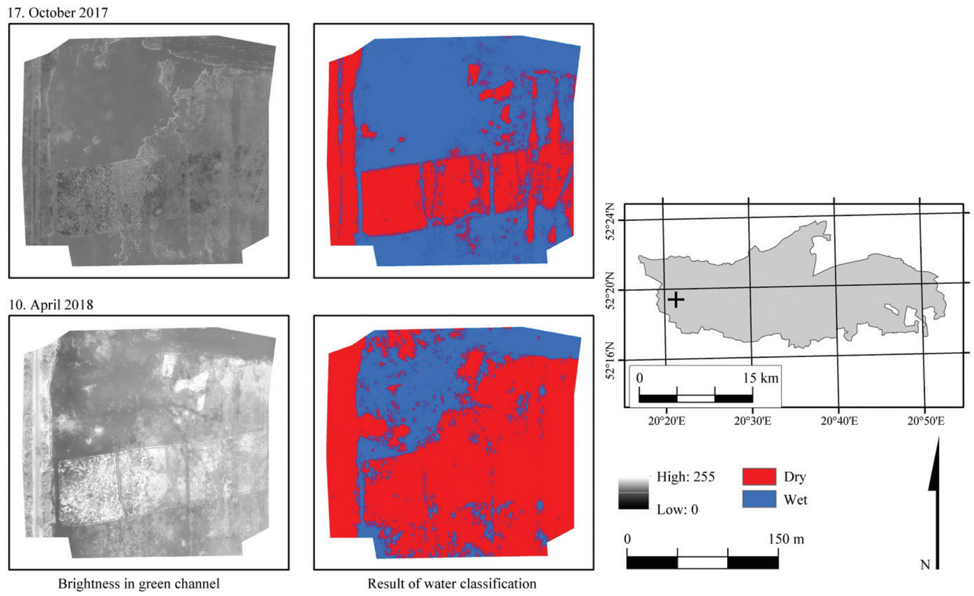

Fig. 3. Wet/dry pixels classification – GTP no. 3

Table 3. Quality indicators for regression results (including the top five) for session

RMSE	Percentage of perfect estimations (0% error)	Percentage of good estimations (<=10% error)	Percentage of tolerable estimations (<=25% error)	Sentinel dataset	Training GTPs	Meta-estimator	R^2-Score [%]
Vernal session - the best results for ROVPs: GTP no. 2, 3, 4							
11.86	35	92	95	NDWI	3, 4	RFR100	30
11.87	35	92	95	NDWI	3, 4	BR100	31
11.93	35	90	95	OPT	3, 4	ETR100	61
11.98	35	89	95	NRGB	3, 4	ETR100	42
12.10	52	92	95	NDWI	3, 4	ETR100	20
Autumnal session - the best results for ROVPs: GTP no. 2, 3, 4							
21.06	10	36	83	OPT	2, 3	RFR100	66
22.04	10	30	83	OPT	2, 3	BR100	66
27.05	41	46	57	NRGB	3, 4	ETR100	43
27.09	41	46	53	OPT	3, 4	BR100	71
27.12	41	45	53	OPT	3, 4	RFR100	70
Autumnal session - the best results for ROVPs: GTP no. 1							
14.67	23	65	89	NRGB	4, 2	ETR100	41
14.90	23	65	89	OPT	4, 2	ETR100	76
17.37	23	64	88	NRGB	4, 2	BR100	39
18.01	23	64	88	NRGB	4, 2	RFR100	38
18.02	23	73	89	NDWI	4, 2	BR100	18
Autumnal session - the best results for ROVPs: GTP no. 6							
24.40	34	52	74	OPT	3, 4	ETR100	75
24.92	34	52	73	NRGB	3, 4	ETR100	43
25.25	34	52	73	OPT	3, 4	BR100	71
25.26	34	52	73	OPT	3, 4	RFR100	70
25.27	34	51	72	NRGB	3, 4	RFR100	43

a set that includes the GTPs 2, 3 and 4 was used, as a learning dataset. The learning dataset was split into two subpopulations: regressor training pixels (RTPs) and regressor inner validation pixels (RIVPs). The pixels of one GTP were not included within the RIVPs and were used as regressor outer validation pixels (ROVPs).

The regression RIVPs were then used for the evaluation of the R^2-score of trained regressor. ROVPs (independent samples) were used for the RMSE evaluation. For the autumnal session, additional RMSEs were calculated using ROVPs from GTPs 1 and 5. As a part of the quality evaluation, differences in the percentage of wet VHR pixels were counted for each meta-estimator used as a regressor and for each Sentinel dataset (Tab. 3).

Tested meta-estimators show a similar distribution of errors measured on the basis of differences between the regressed and observed area of the free water table (ROVPs, Fig. 4). Improved results (characterized by the lowest percentage of wrong estimated pixels) were acquired based on GTPs 3 and 4 than other combinations (Tab. 3, Fig. 4). This is clearly visible in Figure 4, where the distribution of errors is characterized by a relatively low count of considerably large values and with small standard deviations. The worst (characterized by the highest percentage of wrong estimated pixels) result was acquired without GTP 3 as a part of the learning dataset. This is visible as a wide range of inlier points (Fig. 4).

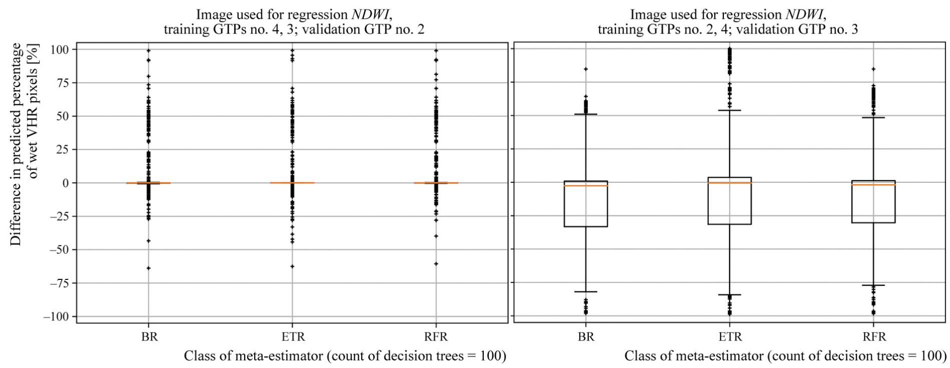

Fig. 4. High (left side) and low (right side) quality estimation for the example of vernal *NDWI* (yellow line – mean, black cross – outliers)

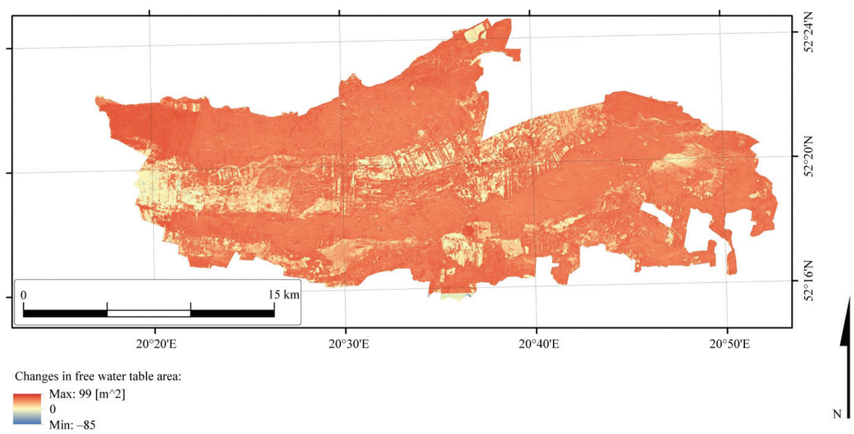

Fig. 5. Changes in the free water table evaluated on the basis of predictions using all Sentinel-2 optical bands and the ETR100 meta-estimator (more detailed description can be found in the text)

2.5. Evaluation of changes in the area of a free water-table

Results characterized by the lowest RMSE and highest R^2-score, described in the previous chapter, were used to evaluate the changes in area of the free water table. In addition, the best results obtained for the vernal session were compared with the best results obtained for the autumnal session by a simple subtraction. Negative values indicate areas where the free water table decreased. Likewise, positive values indicate areas where the free water table increased.

For the comparison, results for all optical bands were used, regressed using the ETR100 meta-estimator, trained by GTPs 3 and 4. Below the resultant map is shown, where 100 m^2 denotes the situation where the LR pixel was completely covered by the free water table in the autumnal session and completely not covered in the vernal session (red pixels, Fig. 5). Likewise, –100 m^2 represents the opposite situation (blue pixels, Fig. 5).

3. Discussion

The spatial accuracy of the prepared UAV orthophotomaps is high (presented in Tab. 1, Fig. 1) and comparable with other papers, such as De Michele et al. (2016), Brokvina et al. (2018) and Chen et al. (2018). The accuracy of water detection at a large scale – using VHR RGB orthophotomaps – is high in comparison to Rokni et al. (2014) and Jones (2015) (Tab. 2).

According to the information given in Table 3, the results of the vernal session are slightly more accurate than for the autumnal session. This is due to plant necromass land coverage, whereby a large part of the wet area was hidden under the plants during the autumnal session. After the partial decomposition, the problem became much less serious. However, this is a considerable limitation for the method applied in this paper.

Significant differences in the used meta-estimator's efficiency were not detected (Fig. 4). Results of the regression acquired using all bands were characterized by similar values of estimation quality. Unexpected low scores gained by predictions based on NDWI in the autumnal session can be caused by low quality satellite data (Tab. 3).

As it can be noticed in Figure 5, the dataset that uses all optical bands may introduce noise, observed as sudden changes of the estimated value along diagonal lines.

4. Conclusion

- VHR orthophotomaps may be an efficient source of ground truth information for water table area regression.
- Meta-estimators, like RFR, ETR and BR, are effective for water table area regression. They provide similar results.
- Satellite images for two acquisitions can be poorly comparable, even if they are characterized by low clouds coverage. This affects the results of the regression.
- The dynamics in plants biomass can be a serious limitation for water detection using optical images. In our experiment, it was shown that post-winter (i.e. vernal) acquisition can be more descriptive compared to pre-winter sessions (i.e. autumnal).

Bibliography

Breiman L., 2001, Random Forests, Machine Learning, 45 (1), 5-32, DOI: 10.1023/A:1010933404324

Brokvina A., Cienciala E., Surový P., Janata P., 2018, Unmanned aerial vehicles (UAV) for assessment of qualitative classification of Norway spruce in temperate forest stands, Geospatial Information Science, 21 (1), DOI: 10.1080/10095020.2017.1416994

Candiago S., Remondido F., De Giglio M., Dubbini M., Gattelli M., 2015, Evaluating multispectral images and vegetation indices for precision farming applications from UAV images, Remote Sensing, 7 (4), 4026-4047, DOI: 10.3390/rs70404026

Chormański J., Okruszko T., Ignar S., Batelaan O., Rebel K.T., Wassen M.J., 2011, Flood mapping with remote sensing and hydrochemistry: A new method to distinguish the origin of flood water during floods, Ecological Engineering, 37 (9), 1334-1349, DOI: 10.1016/j.ecoleng.2011.03.016

Chen R., Chu T., Landivar J., Yang C., Maeda M., 2018, Monitoring cotton (Gossypium hirsutum L.) germination using ultrahigh-resolution UAS images, Precision Agriculture, 19 (1), 161-177, DOI: 10.1007/s11119-017-9508-7

De Michele C., Avanzi F., Passoni D., Barzaghi R., Pinto L., Dosso P., Ghezzi A., Gianatti R., Della Vedova G., 2016, Using a fixed-wing UAS to map snow depth distribution: an evaluation at peak accumulation, The Cryosphere, 10 (2), 511-522, DOI: 10.5194/tc-10-511-2016

Demarchi L., Bizzi S., Piégay H., 2016, Regional hydromorphological characterization with continuous and automated remote sensing analysis on VHR imagery and low-cost resolution LiDAR data, Earth Surface Processes and Landforms, 42 (3), 531-551, DOI: 10.1002/esp.4092

Drusch M., Del Bello U., Carlier S., Colin O., Fernandez V., Gascon F., Hoersch B., Isola C., Laberinti P., Martimort P., Meygret A., Spoto F., Sy O., Marchese F., Bargellini P., 2012, Sentinel-2: ESA's optical high-resolution mission for GMES operational services, Remote Sensing of Environment, 120, 25-36, DOI: 10.1016/j.rse.2011.11.026

Eling C., Wieland M., Hess C., Klingbeil L., Kuhlmann H., 2015, Development and evaluation of a UAV based mapping system for remote sensing and surveying applications, International Archives of the Photogrammetry, Remote Sensing and Spatial Information Sciences, 40, 233-239, DOI: 10.5194/isprsarchives-XL-1-W4-233-2015

Geurts P., Ernst D., Wehenkel L., 2006, Extremely randomized trees, Machine Learning, 63 (1), 3-42, DOI: 10.1007/s10994-006-6226-1

Gislason P., Benediktsson J., Sveinsson J., 2006, Random Forest for land cover classification, Pattern Recognition Letters, 27 (4), 294-300, DOI: 10.1016/j.patrec.2005.08.011

Görn S., Dobner B., Suchanek A., Fischer K., 2013, Assessing human impact on fen biodiversity: effects of different management regimes on butterfly, grasshopper and carabid beetle assemblages, Biodiversity and Conservation, 23 (2), 309-326, DOI: 10.1007/s10531-013-0602-5

Gruszczyński T., Krogulec E., 2012, Wybór wariantu renaturalizacji obszarów podmokłych w Kampinoskim Parku Narodowym na podstawie badań modelowych, Biuletyn Państwowego Instytutu Geologicznego, 451, 45-52

Huang C., Chen Y., Wu J., Li L., Liu R., 2015, An evaluation of Suomi NPP-VIIRS data for surface water detection, Remote Sensing Letters, 6 (2), 155-164, DOI: 10.1080/2150704X.2015.1017664

Jaya N., Nagai M., 2017, Integrated land deformation and groundwater monitoring using Synthetic Aperture Radar (SAR) Interferometry processing, GISRUK, 116, 5 pp.

Jones J., 2015, Efficient wetland surface detection and monitoring via Landsat: Comparison with in situ data from Everglades depth estimation network, Remote Sensing, 7 (9), 12503-12538, DOI: 10.3390/rs70912503

Kopeć D., Michalska-Hejduk D., Krogulec E., 2013, The relationship between vegetation and groundwater levels as an indicator of spontaneous wetland restoration, Ecological Engineering, 57, 242-251, DOI: 10.1016/j.ecoleng.2013.04.028

Krogulec E., Zabłocki S., 2015, Relationship between the environmental and hydrogeological elements characterizing groundwater-dependent ecosystems in central Poland, Hydrogeology Journal, 23 (7), 1587-1602, DOI 10.1007/s10040-015-1273-y

Lagüela S., Diaz-Vilariño L., Roca D., Lorenzo H., 2015, Aerial thermography from low-cost UAV for the generation of thermographic digital terrain models, Opto-Electronics Review, 23 (1), 76-82, DOI: 10.1515/oere-2015-0006

Lipiński J., 2006, Zarys rozwoju oraz produkcyjne i środowiskowe znaczenie melioracji w świetle badań, Acta Scientiarum Polonarum. Formatio Circumiectus, 5 (1), 3-15

Louppe G., Geurts P., 2012, Ensembles on random patches, [in:] Machine Learning and Knowledge Discovery in Databases, ECML PKDD 2012, Lecture Notes in Computer Science, vol. 7523, P.A. Flach, T. De Bie, N. Cristianini (eds.), Springer, Berlin, Heidelberg, 346-361

McFeeters S.K., 1996, The use of the Normalized Difference Water Index (NDWI) in the delineation of open water features, International Journal of Remote Sensing, 17 (7), 1425-1432, DOI: 10.1080/01431169608948714

Pennings S.C., Grant M.-B., Bertness M.D., 2004, Plant zonation in low-latitude salt marshes: disentangling the roles of flooding, salinity and competition, Journal of Ecology, 93 (1), 159-167, DOI: 10.1111/j.1365-2745.2004.00959.x

Pereira J., 1999, A comparative evaluation of NOAA/AVHRR vegetation indexes for burned surface detection and mapping, IEEE Transactions on Geoscience and Remote Sensing, 37 (1), 217-226, DOI: 10.1109/36.739156

Piniewski M., Gottschalk L., Krasovskaia I., Chormański J., 2012, A GIS-based model for testing effects of restoration measures in wetlands: A case study in the Kampinos National Park, Poland, Ecological Engineering, 44, 25-35

Rokni K., Ahmad A., Selamat A., Hazini S., 2014, Water feature extraction and change detection using multitemporal Landsat imagery, Remote Sensing, 6 (5), 4173-4189, DOI: 10.3390/rs6054173

Trandziuk P., 2015, Opracowanie 1 etapu analizy funkcjonowania jazów na Kanale Łasica w KPN, unpublished

Torresan C., Berton A., Carotenuto F., Di Gennaro S.F., Gioli B., Matese A., Miglietta F., Vagnoli C., Zaldei A., Wallace L., 2017, Forestry applications of UAVs in Europe: a review, International Journal of Remote Sensing, 38 (8-10), 2427-2447, DOI: 10.1080/01431161.2016.1252477

Turner D., Lucieer A., Watson C., 2012, An automated technique for generating georectified mosaics from ultra-high resolution Unmanned Aerial Vehicle (UAV) imagery, based on Structure from Motion (SfM) point clouds, Remote Sensing, 4 (5), 1392-1410, DOI: 10.3390/rs4051392

Walker K., Boulton A., Thomas M., Sheldon F., 1994, Effects of water-level changes induced by weirs on the distribution of littoral plants along the River Murray, South Australia, Australian Journal of Marine and Freshwater Research, 45 (8), 1421-1438, DOI: 10.1071/MF9941421

Wang S., Zhuang Q., Yu Z., 2016, Quantifying soil carbon accumulation in Alaskan terrestrial ecosystems during the last 15000 years, Biogeosciences, 13 (22), 6305-6319, DOI: 10.5194/bg-13-6305-2016